Impedance Control of Collaborative Robots Based on a Joint Torque Servo with Active Disturbance Rejection

Tianyu Ren, Yunfei Dong, Dan Wu*, and Ken Chen

***Abstract*—Muscle-skeleton systems as human arms feature variable impedance behavior so that they are applicable to a variety of manipulation tasks, some of which are difficult for current robots. Due to the inherent actuator flexibility and nonlinear friction, the implementation of impedance control on robots generally requires great control efforts. In this paper, a scheme for variable impedance control have been designed and implemented for a 7 degree-of-freedom robot manipulator in a cascading structure consisting of an inner loop torque servo and an outer loop impedance control. An active disturbance rejection controller in the inner loop is designed to reduce the effect of actuator nonlinearity, especially the motor friction and the compliance in transmission system. Results have been given in simulations and experiments in which the proposed joint torque controller with an extended state observer can effectively estimate and compensate for the total disturbance. Based on the satisfactory inner torque servo, a standard PD controller with gravity compensation in the outer loop is employed to achieve variable impedance control in both constrained and unconstrained robot motion. The overall control framework is analytically proved to be stable, and further it is validated in experiments with our robot testbed.**

***Index Terms*—Impedance control, torque feedback, ADRC, ESO, collaborative robot**

I. Introduction

Traditional industrial robots are usually driven by gear-head motors and they are purely stiff positioning devices that preform on specific tasks such as welding, painting, and palletizing (Hogan, 1984). For collaborative robots designed for compliance manipulation, impedance control is preferred for the required interaction between a robot arm and an environment, which demands a robot arm capable of producing accurate joint torques such that the appropriate force is realized at the end-effector (Fiala and Wavering, 1992, Vallery et al., 2008). Actuator dynamics must be considered in such torque-based control methods:

1) Joint torsional flexibility: The most commonly used harmonic reducer is a recognized source of joint flexibility (Hashimoto et al., 1991, Sweet and Good, 1984). In fact, 89% of the torsional compliance of industrial robots is due to compliance of the harmonic drive, by contrast, linkage compliance is insignificant (Rivin, 1985).

2) Motor friction: The motor-side friction and stiction coming from supporting bearings and the input shaft of the reducer could become considerably large with the multiplication of the gear ratio. This can cause undesired behavior, in particular when coupled with integral control (Townsend and Salisbury, 1987), and deteriorate the compliant behavior of the robot.

To address these problems, direct-drive actuators are adopted to supply the required drive torque directly between the two links without gears, which seems ideal for robot actuators (Hollerbach et al., 1993). However, compared with the commonly used actuator consisting of a servo motor and a reducer, currently available direct drive motors can be much bulkier for the same output torque and have larger power dissipation (Hunter et al., 1991). From another point of view, the inner loop torque sensing and control strategy is developed. The torque sensing devices are mounted on the joints of the robot to measure the reducer output torque and provide closed-loop torque control. In early researches, only simple feedback control laws were used in the torque closed loop subject to controller hardware (e.g., PID controller in (Wu, 1985) and (Luh et al., 1983)). In (Albu-Schäffer and Hirzinger, 2001), a torque controller design with the idea of remaining the system passivity was introduced and has been implemented on the DLR’s lightweight robot (Albu-Schaffer et al., 2004, Ott et al., 2004), which is actually a PD controller with model-based parameter setting and can be interpreted as a scaling of the apparent motor inertia. With this passivity-based method in the inner loop, effective damping of the joint oscillations could be achieved. This research result is now widespread in academic communities and also in industrial applications increasingly. However, the joint friction was not considered explicitly in the analysis of robot dynamics and the controller design. In (Hur et al., 2012), a time-delay control (TDC) method was used to control the joint torque and overcome high friction and other unknown disturbances without considering joint flexibility produced by the harmonic reducer. TDC does not require a full analytical description of the robot dynamics, while information about higher order derivatives of the output signals is necessary for this controller. The ATR Lab used a joint torque servo and passivity-based approach for control of arms, legs and torso of their humanoid robot to achieve joint-level compliance (Cheng et al., 2007). In this research, the flexible joint is recognized as a part of the dynamic model and couples with the rigid robot dynamics via the relationship between joint torque and its displacement. This coupling effect results in a fourth-order flexible robot dynamic system and consequently complicates controller design and stability analysis. (See details in section 2.)

Decoupling-based approaches with a partial or full linearization of a closed loop system were considered to achieve the best theoretical performance (Mason, 1981). Taking advantage of the model analysis, it was proven that the robots with elastic joints can be linearized via dynamic feedback (De Luca and Lanari, 1995). Derived from the robot and actuator model, an inner loop nonlinear compensator in the joint torque loop has shown to be effective in the reduction of the motor friction of a PUMA manipulator (Pfeffer et al., 1989). In (Tian and Goldenberg, 1995) and (De Luca and Lucibello, 1998), a two-stage control strategy was employed that consisted of a motion controller and a computed-torque-based joint torque controller by using state feedback laws. This method has no restriction of joint flexibility but relies on an accurate dynamic model and measurement of state variables to ensure effectiveness. To manage uncertainties in the robotic system, adaptive extensions have been developed for most of these controllers (Tian and Goldenberg, 1995, Zhu and De Schutter, 1999). Unfortunately, they are still sensitive to unmodeled dynamics even with enhancements. Singular perturbation-based controllers have simpler control laws for the torque loop and they are easy to implement (Ott et al., 2002, Spong, 1989). Under this conception, the motor torque was divided into a slow part and a fast part, corresponding to the control inputs of the two subsystems of the robot dynamics that may be controlled separately, but the artificial division of the fast and slow parts limited theoretical and practical application to the case of high stiffness joint. In (Kawai et al., 2015) and (Kawai et al., 2016), an integral-proportional differential torque controller based on resonance ratio control was proposed. Joint torque feedback is utilized to suppress the vibration due to joint flexibility. However, careful parameter tuning is needed in this method and the tuning process is not easy.

It is obvious that the existing solutions require either accurate mathematical model of the plant or the measurement of high order derivatives of the robot joint position. Usually, it is more applicable to build a disturbance observer to estimate the model uncertainties and disturbances (Pan et al., 2016). This approach of ADRC, which does not share the problems mentioned above, is represented by an active disturbance rejection concept that features an extended state observer (ESO) for the real-time estimation and compensation of total disturbance (sum of the unknown plant dynamics and the external disturbance) (Gao, 2006a, Han, 2009). It has already proven a promising solution in practice (Przybyła et al., 2012, Wu et al., 2007, Xue et al., 2015, Ren et al., 2018) and an adequate theory in research (Huang and Xue, 2014, Shao and Gao, 2016, Yang and Huang, 2009, Zhou et al., 2009). In our previous work (Ren et al., 2017), we have proposed a torque controller with the idea of disturbance rejection where we focus mainly on the problem of time delay in the actuator and the experiments are restricted to a single joint testbed.

The motivation of our work is to give out a simple yet effective force control scheme for collaborative robot by addressing the problem of disturbance rejection in joint torque. In this paper, a joint torque controller with a linear ESO is used to decouple the joint actuators from the multi-rigid-body system of a constrained robot and compensate for the motor friction. Moreover, in order to realize robot force control, we embed this controller into the impedance control framework.

The main contributions of the presented work is the design of a model-free robot force controller with the ability to reject torque disturbances from robot-actuator coupling effect and motor friction, applicable for both constrained and unconstrained robotic applications. Simulation and experiment results from a 7-DOF robot are given to show the effectiveness of the proposed controller. In section 2, the models of a robot and joint actuators are introduced, and the dominant disturbances in the actuator system are identified. Section 3 begins the discussion of joint torque feedback control by recapitulating the model-based controller and follows with a discussion of ADRC, taking advantage of an extended state observer. Then, the designed joint torque controller is incorporated into an outer loop impedance controller for robot manipulation in section 4. Experimental results are presented to exemplify the controller performance of the proposed impedance control in section 5. Finally, concluding remarks and comments are provided.

II. Problem Statement

A. Description of the Collaborative Robot Testbed

A dexterous collaborative robot arm (DCRA) is developed for industrial and service applications (Fig. 1). It is a seven degrees of freedom (DOF) manipulator that incorporates a torque sensor and link-side encoder at each joint. The joint of DCRA is actuated by a servo motor with its output shaft connected to the wave generator of a harmonic reducer. The flex-spline of the reducer is attached to one end of an analog torque sensor, while the manipulator arm is attached to the other end. In this way, the driving torque between the actuator and the link is gauged directly. The hardware structure of the robot is shown in Fig. 2.

Fig. 1. The experimental single joint manipulator with torque sensing.

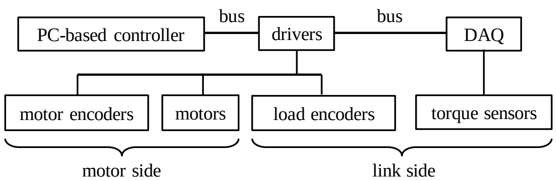

Fig. 2. Hardware structure of the proposed robot controller system.

B. Modeling of a Multi-joint Robot Manipulator

The dynamic model of a n-DOF flexible joint manipulator is given as proposed in (Spong, 1987), consisting of a rigid robot arm (1) and a flexible joint actuator (2)

$$\boldsymbol{M}(\boldsymbol{q})\,\ddot{\boldsymbol{q}} + \boldsymbol{C}(\boldsymbol{q},\dot{\boldsymbol{q}})\,\dot{\boldsymbol{q}} + \boldsymbol{g}(\boldsymbol{q}) = \boldsymbol{\tau} + \boldsymbol{\tau}_{ext}\,, \tag{1}$$

$$\begin{cases} \boldsymbol{B}\ddot{\boldsymbol{\theta}} + \boldsymbol{\tau} = \boldsymbol{\tau}_m - \boldsymbol{\tau}_f \\ \boldsymbol{\tau} = \boldsymbol{K}(\boldsymbol{\theta} - \boldsymbol{q}) \end{cases}, \tag{2}$$

wherein, $\boldsymbol{q} \in \mathbb{R}^n$ and $\boldsymbol{\theta} \in \mathbb{R}^n$ represent the link side and motor side angular positions, respectively, as reflected through the gear ratios. In this way, for the entire robot, each joint becomes a fourth-order system with the state determined by the position and velocity of both motor rotor and link. $\boldsymbol{M}(\boldsymbol{q}) \in \mathbb{R}^{n\times n}$, $\boldsymbol{C}(\boldsymbol{q},\dot{\boldsymbol{q}})\,\dot{\boldsymbol{q}} \in \mathbb{R}^n$ and $\boldsymbol{g}(\boldsymbol{q}) \in \mathbb{R}^n$ are the components of the rigid body model: inertia matrix, centripetal and Coriolis vector, and gravity vector. $\boldsymbol{B}=\mathrm{diag}(B_i) \in \mathbb{R}^{n\times n}$ and $\boldsymbol{K}=\mathrm{diag}(K_i) \in \mathbb{R}^{n\times n}$ are the diagonal, positive definite motor rotor inertia matrices and joint stiffness respectively. $\boldsymbol{\tau}_m \in \mathbb{R}^n$ represents the electromagnetic torque of the motors, and $\boldsymbol{\tau} \in \mathbb{R}^n$ is the joint torque. $\boldsymbol{\tau}_{ext} \in \mathbb{R}^n$ is the external torque acting on the robot joint. $\boldsymbol{\tau}_f \in \mathbb{R}^n$ is the friction torque.

C. Modeling of the Joint Actuator

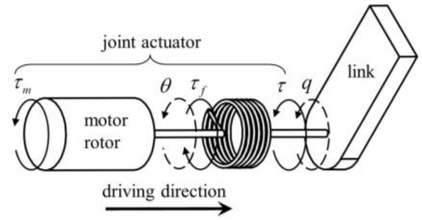

Fig. 3. Schematic model of a typical robot actuator

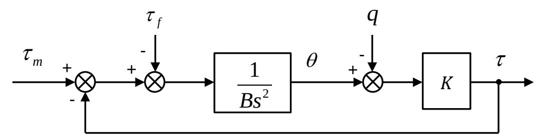

Fig. 4. Block diagram of the joint actuator.

Fig. 3 and Fig. 4 shows the schematic model and the block diagram of a typical robot actuator respectively. It can be represented as a second-order system

$$\ddot{\tau} = (-\frac{K}{B}\tau) + (-\frac{K}{B}\tau_f - K\ddot{q}) + \frac{K}{B}\tau_m \tag{3}$$

where $(-\frac{K}{B}\tau)$ is the actuator dynamics and $(-\frac{K}{B}\tau_f - K\ddot{q})$ is the external disturbance. It is noteworthy that the serial elastic actuator (SEA) (Pratt and Williamson, 1995) has the same representation of Fig. 3, but its stiffness is introduced deliberately to facilitate the position-based control so that it is much lower than that of the flexible joint that we focus on. In the viewpoint of joint torque control, the motion of a robot link q is one of the biggest source disturbances from the robot-environment system acting on the joint actuator, denoted as *Link Motion Disturbance* (LMD). Though it is impossible to predict the link motion when the robot moves in a constrained environment, its changing rate is limited by the robot resonant frequency hinging on the inertia of robot links and the stiffness of joints (Wu, 1985). Experimental results from unconstrained robot motion have shown that the compliance of the electric joint actuator of articulated industrial robot could result in light-damped vibrational modes with resonances typically from 8-12 Hz (Mills, 1992). However, in constrained robot motion (when the robot interact with the environments), the dynamic system will change a lot as the stiffness of the structure is increased. So that in this working condition, the LMD with higher frequency but limited amplitude will be added to the robot joints, which is supposed to be compensated by the same controller. Motor friction τ_f is another significant disturbance which is affected by many factors: temperature, rotation speed and output torque. To understand this problem, we investigated our robot hardware through a static loading experiment in joint 4. The motor torque is derived from the motor winding current, and the actuator output is directly measured by the joint torque sensor (Fig. 5). The Coulomb friction is constant for low torque output, while it decreased when the actuator approaches the rated torque. It is therefore considered as one of the major source of nonlinear disturbance in the problem of robot control. Here, we do not model these disturbances for the presented control algorithms; instead, we use an observer to estimate it in real time and compensate for its negative effects.

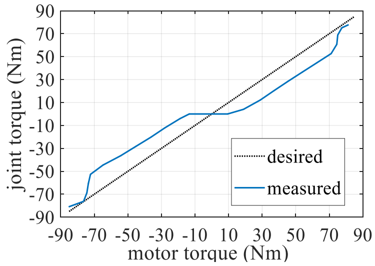

Fig. 5. Relationship between the motor induction torque and actuator output torque in the steady state. The ideal relationship is the dashed line. The solid line is the experimental results of the single joint manipulator.

III. Design of Joint Torque Servo System

A. Identification of the Total Disturbance in the Actuator

The design of the joint torque controller is independent of the manipulator configuration such that a SISO servo algorithm with a wide bandwidth is applicable. From (3), the dynamics of a joint actuator can be rewritten as a second-order integrator:

$$\ddot{\tau} = f(\tau, w) + b\tau_m \tag{4}$$

Herein, $f(\tau,w) = (-\frac{K}{B}\tau) + (-\frac{K}{B}\tau_f - K\ddot{q})$ is considered the total disturbance acting on a linear system where $w = (\tau_f, \ddot{q})$ contains the external perturbation. A good model of f is not always available due to the complex motor friction. $b = K/B$ is a system parameter and it can be calculated from the plant information. In the ADRC framework, it is not necessary to obtain the analytic form of f, but the estimation $\hat{f}$ is obtained in real time (there is no noticeable delay in the observation) through an observer. The ESO originally proposed in (Han, 2009) has been shown to have a great capability of handling different types of disturbances (e.g., constant, square, sinusoidal) without adjusting the structure or parameters (Yang and Huang, 2009), and the magnitude of the observer error monotonically decreases with the observer bandwidth (Zhou et al., 2009).

B. Torque Controller Design with Active Disturbance Rejection

The main idea of an ESO is to use an augmented state space model that includes the unknown $f(\tau,w)$ as an additional state. Then, system (4) can be written in the augmented state space form as

$$\begin{cases} \dot{x}_1 = x_2 \\ \dot{x}_2 = x_3 + b\tau_m \\ \dot{x}_3 = \upsilon \\ y = x_1 \end{cases} \quad \text{with} \quad \begin{cases} x_1 = \tau \\ x_3 = f(\tau, w) \\ \upsilon = \dot{f}(\tau, w) \end{cases}. \tag{5}$$

Then the ESO is able to estimate the plant states. $\boldsymbol{x} = [x_1 \quad x_2 \quad x_3]^T$ is estimated by $\boldsymbol{z} = [z_1 \quad z_2 \quad z_3]^T$ within the observer. Consequently, $\hat{f} = z_3$ is the estimation of the total disturbance f.

$$\begin{cases} e_o = z_1 - \tau \\ \dot{z}_1 = z_2 - \beta_1 e_o \\ \dot{z}_2 = z_3 - \beta_2 e_o + b\tau_m \\ \dot{z}_3 = -\beta_3 e_o \end{cases} \tag{6}$$

where e_o is the estimation error of joint torque, and

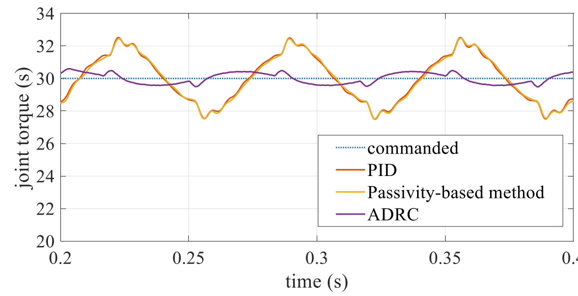

(a)

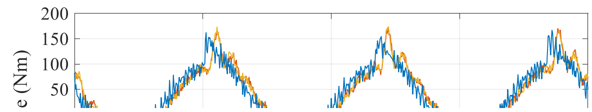

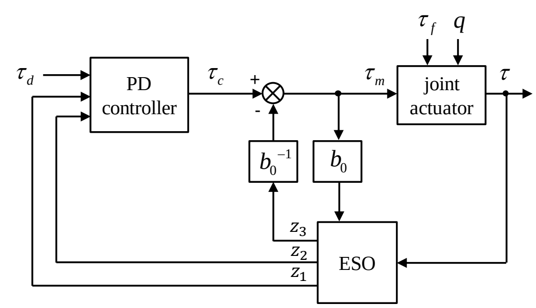

Fig. 6. Architecture of the developed active disturbance rejection controller for joint torque control

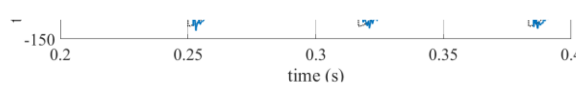

(c)

Fig. 7. Simulation results. (a) Step response of the closed-loop joint torque controllers under motor friction and link motion disturbance. (b) Control signals of both controllers for the disturbed system. (c) The real-time estimation of the total disturbance by the ESO.

$\beta_1, \beta_2, \beta_3$ are the gains of the observer parameterized by using a simple pole-placement method as proposed in (Gao, 2006b):

$$\beta_1 = 3\omega_o, \beta_2 = 3\omega_o^2, \beta_3 = \omega_o^3 \tag{7}$$

Where ω_o is the observer bandwidth that is restricted by noise amplitude in the feedback channel and it is usually determined though experiment (Gao, 2006b). Along with the disturbance estimation $\hat{f}$ from the ESO, a controller is designed to guarantee trajectory tracking with the cancellation of the total disturbance. The governing signal is defined as follows.

$$\tau_m = \tau_c - \frac{\hat{f}}{b} \tag{8}$$

In the proposed torque feedback system, a PD controller was chosen, and the control law is thus written as

$$\tau_c = k_p\left(\tau_d - z_1\right) - k_d z_2 \tag{9}$$

k_p and k_d are the gains of the feedback controller and parameterized as (Gao, 2006b):

$$k_p = \frac{\omega_c^{\ 2}}{b}, k_d = \frac{2\omega_c}{b}. \tag{10}$$

wherein ω_c is the bandwidth of the closed-loop system and can be tuned as a regular PD controller (Gao, 2006b). High bandwidth can cause better tracking performance and reduce the apparent motor inertia observed at the output of the actuator. However, this will lead to severe actuator saturation and make the system sensitive to the torque sensor noise. Finally, an active disturbance rejection controller has been established for the robot joint torque servo and its architecture is illustrated in Fig. 6. Based on the assumption that f is sufficiently compensated by the ESO, the closed-loop elastic joint is reduced to a double integrator, and furthermore, according to the theorem in (Khalil, 2014), the system is finite-gain $\mathcal{L}_2$ stable. These results are consolidated by (Zhou et al., 2009) and (Shao and Gao, 2016) based on singular perturbation analysis, in which there is a $\omega_o^* > 0$, such that for all $\omega_o > \omega_o^*$ the ADRC system is exponentially stable as $\omega_o \to \infty$.

C. *Simulation and comparison with existing methods*

The ability of disturbance estimation makes the ADRC strategy adaptive to actual robot system subjected to even unknown disturbances other than those given in Sec. II-C. Here a simulation environment with synthetic disturbance is preferred to illustrate the performance of the ESO. A comparison in performance between the proposed method and the other two practical torque controllers: a classic PID controller and the passivity-based method used by DLR robots (Albu-Schäffer et al., 2007), is provided by simulation results.

Parameters of the simulation model are specified in accordance with the 4th joint of the robot in Table I. A composed disturbance signal is designated carefully to simulate the real situation: a link motion of $q(t) = \frac{\tau_{mc}}{K}\sin(15 \cdot 2\pi t)$ (considering the robot resonant frequency in (Wu, 1985)), and a motor side friction of $\tau_f(t) = \mathrm{sign}(\dot{q}(t)) \cdot (\tau_{fv}\left|\dot{q}(t)\right| + \tau_{fc})$ with $\tau_{fv} = 2$ Nm and $\tau_{fc} = 20$ Nm (take the model of coulomb and viscous friction from (Kelly and Llamas, 1999)). In addition, a random signal with uniform distribution within the range of 0.1 Nm (corresponding to the sensor noise and the filter used for signal processing) is introduced to the feedback signal of the torque sensor. In the conditions above, the controller systems

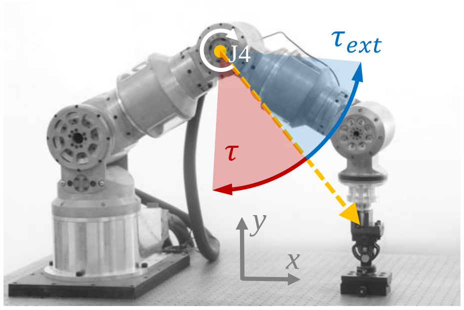

Fig. 8. The manipulator is commanded to exert torques on the environment according to the reference signal in joint torque control mode.

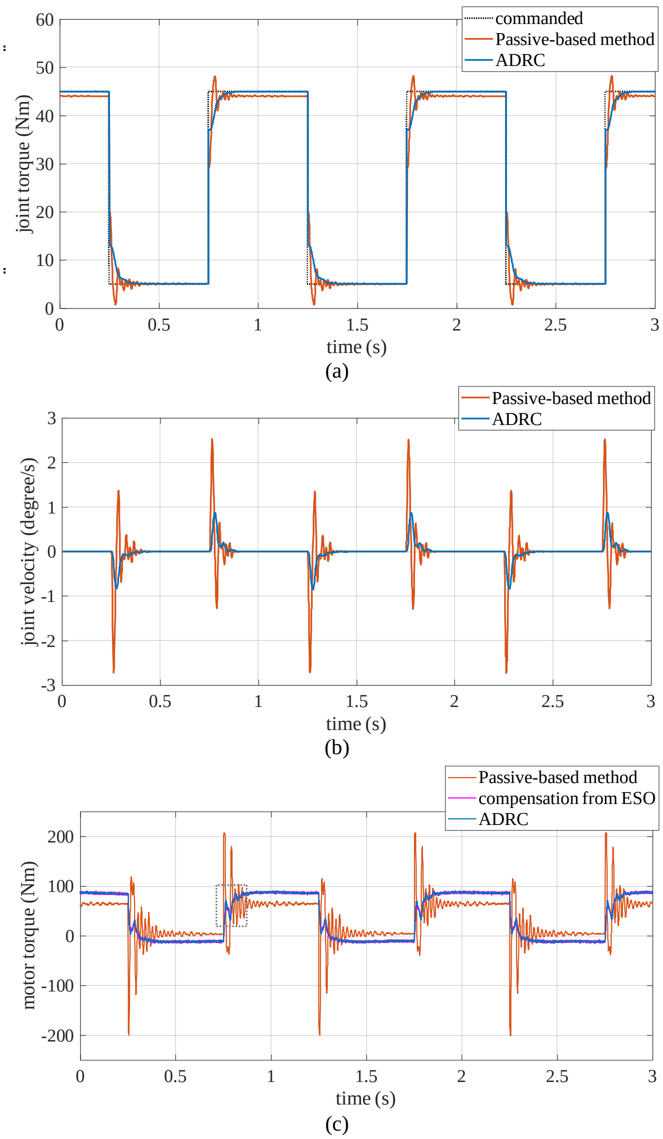

Fig. 9. System response of the passive-based method and ADRC to square wave input. (a) Joint torque. (b) Joint velocity. (c) Motor torque.

are used to follow a reference signal of τ_d=30 Nm under the effect of the total disturbance. All controllers are tuned to provide the best performance according to the systematic approach [45](Wang et al., 1999). The proportional, integral and differential gains of PID are chosen as 50, 150 and 1. In ADRC, ω_c is determined based on the system bandwidth requirement and it is selected to be 350 rad/s. For the passive-based controller, it share the same PD parameters with ADRC. By trading off between the rapidity and the sensor noise robustness, the bandwidth ω_0 of ESO is set to be 1800 rad/s . Comparison of the joint torque achieved for the three controllers is shown in Fig. 7 (a). In Fig. 7 (b), the control signals (motor torque) generated by the controllers are presented.

For ADRC, the shape of the control signal is slightly rugged, while it does not significantly differ from that of others. On the other hand, the difference in the phase between the three controllers is noticeable. With the compensation effect from the ESO, the ADRC react more swiftly (see Fig. 7 (b)). The controller systems of PID and the passivity-based method are obviously subjected to LMD and motor friction, while the system improved by ESO tracked the commanded torque with satisfactory results. In the first raw of Table II, the *Robustness to Total Disturbance* (RTD) of the three controllers (Fig. 7 (c)) that is defined as the ratio of the fluctuation range of the output torque and the amplitude of total disturbance is quantitatively compared. Although there is no prior knowledge of the model and perturbation, ESO gives a satisfying reaction the total disturbance in the actuator.

The simulation is set up at a workstation with a clock speed of 3501 MHz and a RAM of 24 GB. The sample time of the simulation is chosen as the cycle time of DCRA, 250 μs. From the report of computational time in Table II, we can see that all of the three torque controllers are fast enough to satisfy the requirement of real-time control. The time consuming of ADRC is slightly higher than PID but lower than the passive-based method.

D. *Experimental verification*

In this experiment, we tested the proposed torque controller with the fourth joint of the 7-DOF manipulator(Fig. 8). The robot presses its end effecter (EE) onto a fixture with a desired torque. The reference signals are chosen as a square wave and harmonic wave. The performance comparison between the passive-based method and ADRC is shown in Fig .9 and Fig. 10. Both of the controllers are tuned to give a moderate performance on response rapidity, steady-state error and stability to disturbances.

As a multi-rigid system with bilateral support, the robot body is activated by the input torque with a resonant frequency of 40-50 Hz. Therefore, LMD with the same frequency is introduced to the joint torque controllers. Fig. 9 (a) and (b) show that the actuated link produces an impulse link velocity which further leads to an overshoot in joint torque. By contrast, ADRC gives a much better result:

a) LMP compensation: The interaction between the actuators and rigid robot can lead to oscillations in both joint torque and link displacement with high frequency beyond the closed-loop dynamics of the actuator hardware. On the other hand, the ESO usually has a higher bandwidth than the closed-loop system so that it is capable to react to these LMD and suppress system vibration.

b) Motor friction compensation: The detrimental effect of motor friction is mainly compensated locally by the high-bandwidth ESO in ADRC, instead by the whole closed-loop of the passive-based method. When the motor rotor is going to switch its direction to follow the step input (Fig .7 (a)), it is blocked by a stiction. The ESO is able to detect this disturbance and generate spike-like signal to compensate it (Fig .7 (c)) without participation of the PD controller. Therefore, despite nonlinear disturbances, the behavior of the ADRC system is closed to a linear system with predictable performance.

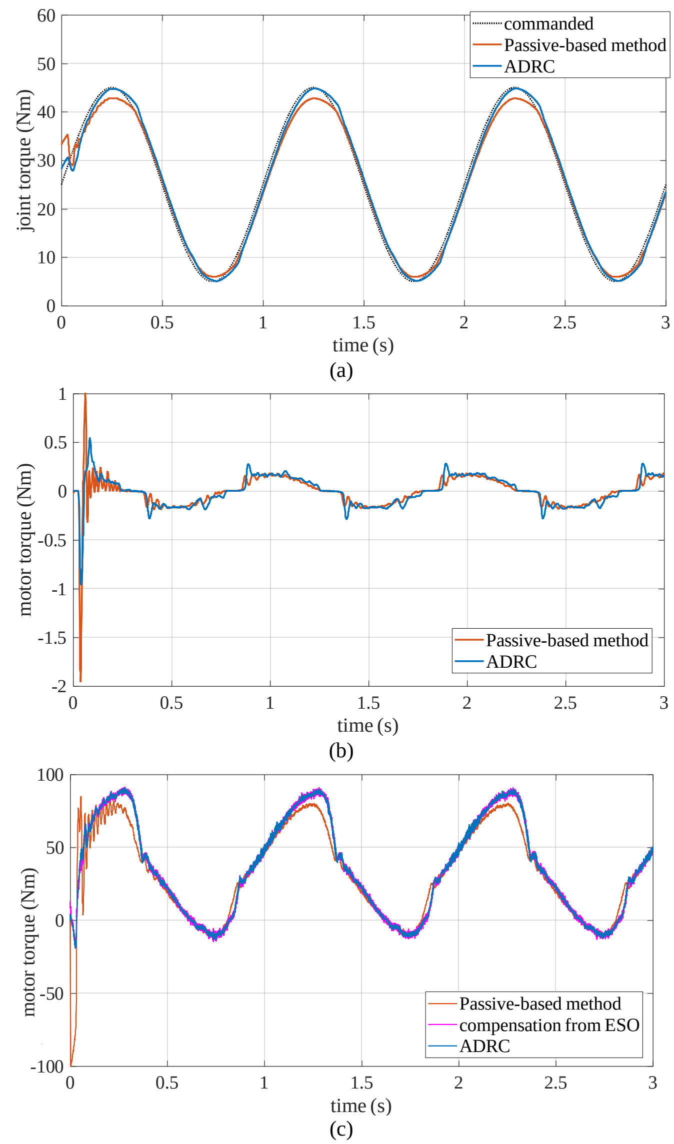

Fig. 10. System response of the passive-based method and ADRC to harmonic wave input. (a) Joint torque. (b) Joint velocity. (c) Motor torque.

c) Steady-state error: It is clear that there exists a steady-state error in the output of the passive-based method due to the inaccurate torque constant of the motor hardware (calibrated, but with error). In ADRC, however, small deviation of from the reference signal is accumulated in ESO as a disturbance and finally eliminated by the controller (Han, 2009).

The same result can be found in the experiment of harmonic signal tracking (Fig. 10). It is noteworthy that the PID controller is now removed from the comparison because it shows almost the same performance as the passive-based controller as presented in the simulation result in the previous section (Fig. 7 (a)). Though the response speed constrained by hardware is similar, ADRC gives a much more stable output with better precision.

IV. Torque-based Variable Impedance Control

A. A Framework for Variable Impedance Control

With the proposed joint torque controller, the complex flexible joint robot system described by (1) and (2) can be expressed as a cascaded system consisting of a rigid robot body and n closed-loop actuators, thus simplifying the design of the robot controller. Based on the elimination of the total disturbance in joint torque, the complete n-DOF manipulator model can be described in the form of state space as

$$\begin{cases} \dot{\boldsymbol{v}} = Dynmc(\boldsymbol{v}, \boldsymbol{\tau} + \boldsymbol{d}_1) \\ \varepsilon^2 \dot{\boldsymbol{w}} = \boldsymbol{A}\boldsymbol{w} + \boldsymbol{B}[\boldsymbol{\tau}_d + \boldsymbol{d}_2] \\ \boldsymbol{\tau} = \boldsymbol{C}\boldsymbol{w} \end{cases} \tag{11}$$

with

$$Dynmc(\boldsymbol{v}, \boldsymbol{\tau} + \boldsymbol{d}_1) = \begin{bmatrix} \dot{\boldsymbol{q}} & \boldsymbol{M}(\boldsymbol{q})^{-1}[\boldsymbol{\tau} + \boldsymbol{d}_1 - \boldsymbol{C}(\boldsymbol{q}, \dot{\boldsymbol{q}})\dot{\boldsymbol{q}} - \boldsymbol{g}(\boldsymbol{q})] \end{bmatrix}^T .$$

$$\boldsymbol{A} = \begin{bmatrix} 0 & \varepsilon^2 \boldsymbol{I}_n \\ -\boldsymbol{\Omega}_{c0}{}^2 \boldsymbol{I}_n & -2\boldsymbol{\Omega}_{c0}\varepsilon \boldsymbol{I}_n \end{bmatrix} \in \mathbb{R}^{2n\times 2n} , \quad \boldsymbol{B} = \begin{bmatrix} 0 \\ \boldsymbol{\Omega}_{c0}{}^2 \end{bmatrix} \in \mathbb{R}^{2n\times n} ,$$

$$\boldsymbol{C} = \begin{bmatrix} \boldsymbol{I}_n & 0 \end{bmatrix} \in \mathbb{R}^{n\times 2n} , \ \boldsymbol{\Omega}_{c0} = \mathrm{diag}(\omega_{c0,i}) \in \mathbb{R}^{n\times n} .$$

Where $\omega_{c0,i}$ is defined as a preset bandwidth of the i-th robot actuator and based on it we can scale the effective bandwidth $\omega_{c,i}$ in (10) with scalar ε : $\omega_{c,i} = \omega_{c0,i} / \varepsilon$ that is the actual bandwidth of the closed-loop system. Vectors $\boldsymbol{v} = \begin{bmatrix} \boldsymbol{q} & \dot{\boldsymbol{q}} \end{bmatrix}^T \in \mathbb{R}^{2n}$ and $\boldsymbol{w} = \begin{bmatrix} \boldsymbol{\tau} & \dot{\boldsymbol{\tau}} \end{bmatrix}^T \in \mathbb{R}^{2n}$ respectively represent the state variables of the rigid robot and actuating systems.

The two disturbances, $\boldsymbol{d}_1, \boldsymbol{d}_2 \in \mathbb{R}^n$, have definite physical significance. $\boldsymbol{d}_1$ contains the perturbation torque coming from the external environment as well as the disturbance beyond the regulating capacity of ADRC. $\boldsymbol{d}_2$ is the disturbance input of the closed-loop actuators consisting of the noise from joint encoders and torque sensors and the compensation error of robot gravity. The design of the outer loop controller ensures that the input/output mapping from $\boldsymbol{d}_1, \boldsymbol{d}_2$ to $\boldsymbol{v}$ is finite-gain $\mathcal{L}_2$ stable with the $\mathcal{L}_2$ gain less than a given tolerance $\sigma > 0$.

To simplify the controller design of the feedback connection system, first assume $\varepsilon = 0$ as (Khalil, 2014), that is, $\omega_{c,i} \to \infty$. Then, the actuator dynamics are neglected, and we have

$$\boldsymbol{\tau} = \boldsymbol{\tau}_d + \boldsymbol{d}_2 . \tag{12}$$

Substituting (12) into the first equation in (11), a dimensionality reduction model is obtained.

$$\dot{\boldsymbol{v}} = Dynmc(\boldsymbol{v}, \boldsymbol{\tau}_d + \boldsymbol{d}), \ \boldsymbol{d} = \boldsymbol{d}_1 + \boldsymbol{d}_2 \tag{13}$$

The state vector $\boldsymbol{v}$ is measured directly by encoders at the link side. In both contact and noncontact robot manipulations,

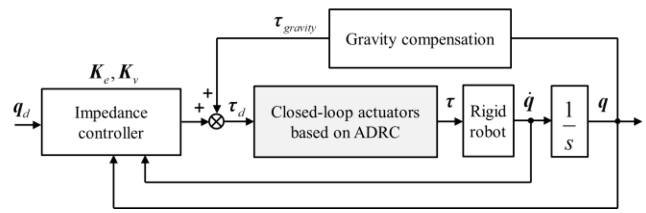

Fig. 11. The overall control structure for both position and impedance control

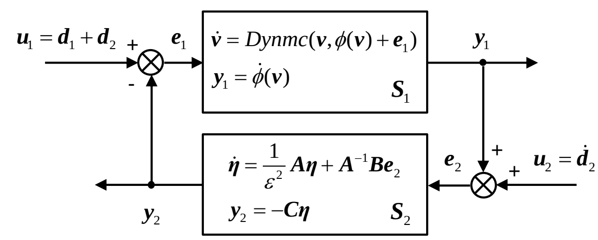

Fig. 12. The feedback connection of the PD controlled rigid robot (S1) and the closed-loop joint actuators with active disturbance rejection (S2).

a PD feedback control law has been proved to produce stable behavior (Anderson, 1990, Kelly, 1997). To achieve a unified structure, a PD controller with gravity compensation is used for the simplified model (Fig. 11)

$$\boldsymbol{\tau}_d = \phi(\boldsymbol{v}) = \boldsymbol{K}_e\tilde{\boldsymbol{q}} - \boldsymbol{K}_v\dot{\boldsymbol{q}} + \boldsymbol{\tau}_{gravity} , \ \tilde{\boldsymbol{q}} = \boldsymbol{q}_d - \boldsymbol{q} . \tag{14}$$

$\boldsymbol{K}_e = \mathrm{diag}(K_{e,i}) \in \mathbb{R}^{n\times n}$ and $\boldsymbol{K}_v = \mathrm{diag}(K_{v,i}) \in \mathbb{R}^{n\times n}$ are stiffness matrix and damping matrix in joint space. $\boldsymbol{\tau}_{gravity} = \boldsymbol{g}(\boldsymbol{q})$ provides model-based compensation for the effect of gravity. Substituting $\phi(\boldsymbol{v})$ into the dimensionality reduction model in (13), we have the dynamic system:

$$\boldsymbol{M}(\boldsymbol{q})\ddot{\boldsymbol{q}} + \boldsymbol{C}(\boldsymbol{q}, \dot{\boldsymbol{q}})\dot{\boldsymbol{q}} = \boldsymbol{K}_e\tilde{\boldsymbol{q}} - \boldsymbol{K}_v\dot{\boldsymbol{q}} + \boldsymbol{d} . \tag{15}$$

A Lyapunov function chosen as

$$V(\boldsymbol{q}, \dot{\boldsymbol{q}}) = \frac{1}{2}\dot{\boldsymbol{q}}^T\boldsymbol{M}(\boldsymbol{q})\dot{\boldsymbol{q}} + \frac{1}{2}\tilde{\boldsymbol{q}}^T\boldsymbol{K}_e\tilde{\boldsymbol{q}} . \tag{16}$$

Obviously, $V(\boldsymbol{q}, \dot{\boldsymbol{q}}) \ge 0$ is a semidefinite function. Then, its derivative with respect to time is calculated.

$$\dot{V}(\boldsymbol{q}, \dot{\boldsymbol{q}}) = \dot{\boldsymbol{q}}^T\boldsymbol{d} - \dot{\boldsymbol{q}}^T\boldsymbol{K}_v\dot{\boldsymbol{q}} . \tag{17}$$

So, we have $\boldsymbol{d}^T\dot{\boldsymbol{q}} = \dot{V}(\boldsymbol{q}, \dot{\boldsymbol{q}}) + \dot{\boldsymbol{q}}^T\boldsymbol{K}_v\dot{\boldsymbol{q}}$, wherein $\dot{\boldsymbol{q}}^T\boldsymbol{K}_v\dot{\boldsymbol{q}} > 0, \ \forall\dot{\boldsymbol{q}} \ne 0$, and further the mapping of $\boldsymbol{d} \to \dot{\boldsymbol{q}}$ is strictly passive for output, which is in agreement with the conclusions in (Anderson, 1990). Let $\delta = \lambda_{\min}(\boldsymbol{K}_v)$, then $\delta > 0$, and we have

$$\begin{aligned} \dot{V}(\boldsymbol{q}, \dot{\boldsymbol{q}}) &\le \boldsymbol{d}^T\dot{\boldsymbol{q}} - \delta\dot{\boldsymbol{q}}^T\dot{\boldsymbol{q}} \\ &= \frac{1}{2\delta}(\boldsymbol{d} - \delta\dot{\boldsymbol{q}})^T(\boldsymbol{d} - \delta\dot{\boldsymbol{q}}) + \frac{1}{2\delta}\boldsymbol{d}^T\boldsymbol{d} - \frac{\delta}{2}\dot{\boldsymbol{q}}^T\dot{\boldsymbol{q}} . \\ &\le \frac{\delta}{2}(\frac{1}{\delta^2}\boldsymbol{d}^T\boldsymbol{d} - \dot{\boldsymbol{q}}^T\dot{\boldsymbol{q}}) \end{aligned} \tag{18}$$

Therefore, we know from the lemma in (Khalil, 2014) that the dimension reduction system is finite-gain $\mathcal{L}_2$ stable.

$$\|\dot{\boldsymbol{q}}\|_{\mathcal{L}_2} \le \gamma_0 \|\boldsymbol{d}\|_{\mathcal{L}_2} + \varsigma_0 \ \text{with} \ \gamma_0 = \frac{1}{\delta} , \ \delta = \lambda_{\min}(\boldsymbol{K}_v) . \tag{19}$$

If $\gamma_0 < 1$, the closed-loop dimension reduction system is

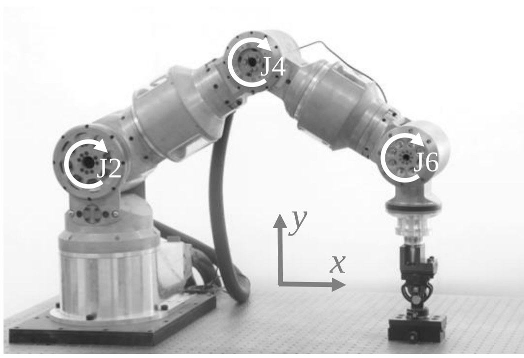

Fig. 13. 2D peg-in-hole manipulation by the DRCA robot enhanced by impedance controller

strictly passive for both input and output (Van der Schaft, 2016). The same control law is applied to the actual system with actuator dynamics, and the entire closed-loop system can be expressed as shown in Fig. 10. The corresponding actual robot system dynamics are described as

$$\begin{cases}\dot{\boldsymbol{v}} = Dynmc(\boldsymbol{v}, \boldsymbol{C}\boldsymbol{w} + \boldsymbol{d}_1) \\ \varepsilon^2 \dot{\boldsymbol{w}} = \boldsymbol{A}\boldsymbol{w} + \boldsymbol{B}[\phi(\boldsymbol{v}) + \boldsymbol{d}_2]\end{cases} \tag{20}$$

With the parametrization of $\boldsymbol{K}_e$ and $\boldsymbol{K}_v$, the robot can display corresponding compliant behaviors to adapt different tasks. Typically, the robot is required to display stiff behavior in directions of motion, while displaying compliant behavior in directions of forces.

B. Input and Output Stability Analysis of the Proposed Framework

To facilitate the analysis, we assume that $\boldsymbol{d}_2$ is differentiable, which is reasonable in real systems with filtered sensor signals. Then a variable substitution is performed as follows:

$$\boldsymbol{\eta} = \boldsymbol{w} + \boldsymbol{A}^{-1}\boldsymbol{B}[\phi(\boldsymbol{v}) + \boldsymbol{d}_2] \tag{21}$$

Using the new variable $\boldsymbol{\eta}$, the actual robot system (20) is rewritten as an equivalent robot system.

$$\begin{cases}\boldsymbol{S}_1:\ \dot{\boldsymbol{v}} = Dynmc(\boldsymbol{v}, \phi(\boldsymbol{v}) + \boldsymbol{d}(t) + \boldsymbol{C}\boldsymbol{\eta}) \\ \boldsymbol{S}_2:\ \varepsilon^2 \dot{\boldsymbol{\eta}} = \boldsymbol{A}\boldsymbol{\eta} + \varepsilon^2 \boldsymbol{A}^{-1}\boldsymbol{B}[\dot{\phi}(\boldsymbol{v}) + \dot{\boldsymbol{d}}_2]\end{cases} \tag{22}$$

It can also be presented as a block diagram, as a feedback connection of two subsystems (Fig. 12).

$\boldsymbol{S}_1$ is the closed-loop system of the rigid robot controlled by a PD controller with gravity compensation in real time, which is one of the simplest position controllers for robot manipulators on which numerous studies have been performed. It has been verified that $\boldsymbol{S}_1$ has a unique equilibrium (Kelly, 1997).

$$\begin{bmatrix}\tilde{\boldsymbol{q}}^* & \dot{\boldsymbol{q}}^*\end{bmatrix}^T = \begin{bmatrix}-\boldsymbol{K}_e^{-1}\boldsymbol{e}_1 & 0\end{bmatrix}^T \tag{23}$$

Herein, $\boldsymbol{e}_1$ is the disturbance input of $\boldsymbol{S}_1$ and $\dot{\phi}(\boldsymbol{v})$ the output added to $\boldsymbol{S}_2$

$$\dot{\phi}(\boldsymbol{v}) = -\boldsymbol{K}_e\dot{\boldsymbol{q}} - \boldsymbol{K}_v\boldsymbol{M}(\boldsymbol{q})^{-1}[\boldsymbol{e}_1 + \boldsymbol{K}_e\tilde{\boldsymbol{q}} - \boldsymbol{K}_v\dot{\boldsymbol{q}} - \boldsymbol{C}(\boldsymbol{q},\dot{\boldsymbol{q}})\dot{\boldsymbol{q}}] + \frac{\partial \boldsymbol{g}(\boldsymbol{q})}{\partial \boldsymbol{q}}\dot{\boldsymbol{q}}. \tag{24}$$

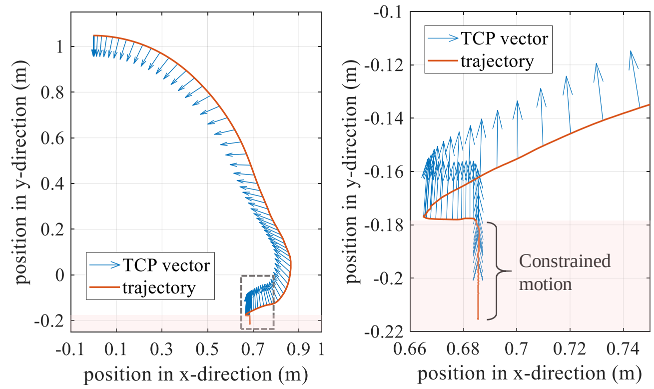

Fig. 14. TCP trajectory and orientation in Cartesian space during the peg-in-hole manipulation

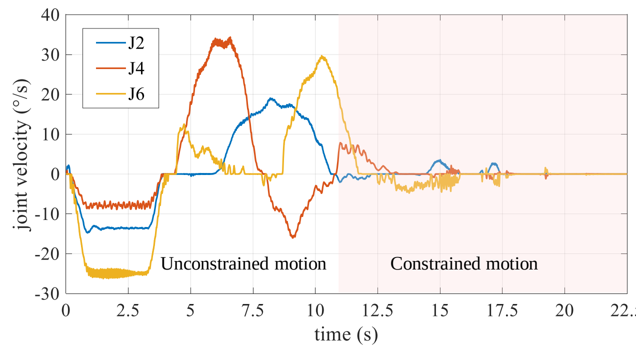

Fig. 15. Robot velocities in joint space during the peg-in-hole manipulation

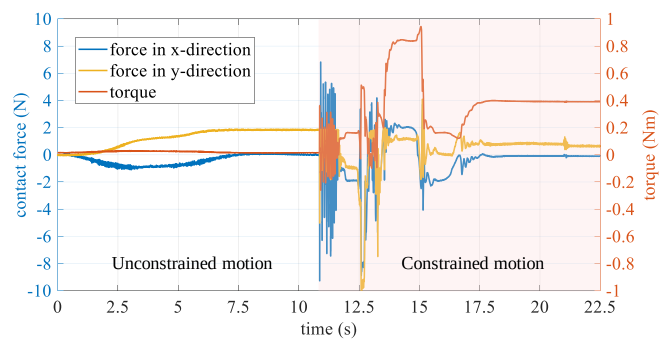

Fig. 16. Contact forces and torque in Cartesian space during the peg-in-hole manipulation

Considering (23), we have $(\boldsymbol{e}_1 + \boldsymbol{K}_e\tilde{\boldsymbol{q}}) \to 0$ when the system comes to equilibrium. In addition, there exists a positive constant k_C meeting $\|\boldsymbol{C}(\boldsymbol{q},\dot{\boldsymbol{q}})\| \le k_C\|\dot{\boldsymbol{q}}\|$. Therefore, (24) is simplified, and the following relationship is derived

$$\|\dot{\phi}(\boldsymbol{v})\| \le c\|\dot{\boldsymbol{q}}\| \text{ with } \begin{aligned} c = {} & \lambda_{\max}(-\boldsymbol{K}_e + \boldsymbol{M}(\boldsymbol{q})^{-1}\boldsymbol{K}_v^2) \\ & + \lambda_{\max}(\boldsymbol{M}(\boldsymbol{q})^{-1})\lambda_{\max}(\boldsymbol{K}_v)k_C + \lambda_{\max}\left(\frac{\partial \boldsymbol{g}(\boldsymbol{q})}{\partial \boldsymbol{q}}\right)\end{aligned}. \tag{25}$$

The inequalities (25) and (19) imply that subsystem $\boldsymbol{S}_1$ is finite-gain $\mathcal{L}_2$ stable

$$\|\boldsymbol{y}_1\|_{\mathcal{L}_2} = \|\dot{\phi}(\boldsymbol{v})\|_{\mathcal{L}_2} \le \gamma_1\|\boldsymbol{e}_1\|_{\mathcal{L}_2} + \varsigma_1 \text{ with } \gamma_1 = \frac{c}{\delta}. \tag{26}$$

$\boldsymbol{S}_2$ represents the effect of the closed-loop actuator dynamics on the nominal rigid robot system. $\boldsymbol{A}$ is Hurwitz as it is the simple superposition of the state matrices of n closed-loop actuators. Then, the finite-gain $\mathcal{L}_2$ stability of $\boldsymbol{S}_2$ is confirmed (Khalil, 2014). So we have

$$\|\boldsymbol{y}_2\|_{\mathcal{L}_2} \le \varepsilon^2\gamma_2 \|\boldsymbol{e}_2\|_{\mathcal{L}_2} + \varsigma_2 \tag{27}$$

with

$$\gamma_2 = 2\lambda_{\max}^2(\boldsymbol{P}) \frac{\|\boldsymbol{A}^{-1}\boldsymbol{B}\|\|\boldsymbol{C}\|}{\lambda_{\min}(\boldsymbol{P})}. \tag{28}$$

Where $\boldsymbol{P}$ is the solution of the Lyapunov equation $\boldsymbol{PA}+\boldsymbol{A}^T\boldsymbol{P}=-\boldsymbol{I}$. If $\varepsilon^2\gamma_1\gamma_2<1$, the stable relationship between the input and output from $(\boldsymbol{d}_1, \boldsymbol{d}_2)$ to $\dot{\boldsymbol{q}}$ in the equivalent system (22) is established. Eventually, we have

$$\|\dot{\boldsymbol{q}}\|_{\mathcal{L}_2} \le \frac{\gamma_0}{1-\varepsilon^2\gamma_1\gamma_2}[\|\boldsymbol{d}\|_{\mathcal{L}_2} + \varepsilon^2\gamma_2\|\boldsymbol{d}\|_{\mathcal{L}_2} + \varepsilon^2\gamma_2\varsigma_1 + \varsigma_2] + \varsigma_0. \tag{29}$$

In this framework, ε decreases as the joint closed-loop bandwidth ω_c increases, which shapes the weight of the actuator dynamics in the whole robot system. Especially when ε decreases to zero, the right side of (29) becomes $\gamma_0\|\boldsymbol{d}\|_{\mathcal{L}_2} + (\varsigma_0+\gamma_0\varsigma_2)$. Here, a significant conclusion is made: the feedback controller designed for the rigid robot is applicable to the actual system with a sufficiently large ω_c. Moreover, the upper bound of $\mathcal{L}_2$ gain remains unchanged, and the passivity of the dimensionality reduction system (13) is reserved for the actual system (20) such that the manipulator will be stable in contact with passive environments and have asymptotically stable joint velocities when contacting arbitrary environments (Anderson, 1990).

V. EXPERIMENT AND RESULTS

A typical robotic assembly task includes robot motion in both unconstrained and constrained environment, and it can lead to complex contacts while in operation. Therefore, it is an ideal practical task to test the effectiveness and stability of the proposed controller. The peg-in-hole task has previously been implemented by using an industrial robot and a compliant F/T sensor. In this experiment, the DRCA robot is commanded to insert a shaft (aluminum alloy) into a slot with corresponding cross section (steel), which is a 2D peg-in-hole problem (Fig. 13). The joint 2, 4 and 6 are used for this task, and their stiffness are chosen empirically as 300 Nm/rad, 150 Nm/rad and 30 Nm/rad, respectively. According to the repositioning precision of the robot, the diameter clearance between the peg and hole is toleranced to 0.2 mm. The trajectory of the task is taught directly by human. Then, the robot moves according to the demonstrated trajectory with the proposed impedance controller and meanwhile the feedback signals from the position and force sensors are recorded.

Fig. 14 is showing the trajectory and orientation of the end effector of the robot in assembly plane. In the first phase, the tool center point (TCP) approaches the position of hole in free space with a relatively high speed. When it contacts with the upper surface of the hole, the robot system gets into the phase of constrained motion in y-direction. As the peg sliding into the hole, the robot losses the other two DOFs of x-motion and rotation, and regains the motion in y-direction. During these two phase as well as the transient process, the robot velocities in joint space keep stable and no severe breaks in velocity signals are observed (Fig. 15). Fig. 16 shows the contact forces and torque in assembly plane measured by the F/T sensor. Slow force changes of in the phase of unconstrained motion are due to gravity while the dramatic force changes at the beginning of constrained motion result from the friction between the robot end and the upper surface of the hole (the lateral motion shown on the right in Fig. 14). In accordance to the results of stable analysis in Sec. IV-B, the robot is in continuous contact with the hole wall with stable force during the insertion. The reasons for the remaining contact force at the end of insertion are the robot positioning error and the high stiffness of the objects.

VI. CONCLUSIONS

A new, cascading approach to variable impedance control for flexible joint robots is presented in this work. Based on only the directly available joint torque signals, the proposed joint torque controller can properly track the reference signals while actively negating disturbance without explicit modeling of the plant or perturbations. Analysis and simulation results show that the ESO enclosed in the joint controller can effectively estimate the total disturbance and compensate for it, which, in this case, is the sum of actuator dynamics, link motion disturbance, motor frictions, and other unmodeled perturbations. Consequently, the closed-loop joint actuators become much closer to ideal torque sources. On the basis of the well-tuned joint torque servo systems, a simple outer loop is designed for impedance control of multi-joint robot. The stability of the double closed-loop system is analyzed with an input and output method, and the result shows that the system is robust against model uncertainties related to robot dynamics, payload changes, and the trivial torque error from the inner loop. Performance of the proposed controller is evaluated in an experiment on our collaborative robot, in which the robot successfully assembles the high stiffness parts. It is remarkable that the proposed impedance controller is easy to implement on robot systems.

VII. APPENDIX FOR ABBREVIATIONS

Abbreviation	Definition
ADRC	Active Disturbance Rejection Control
ESO	Extended State Observer
DOF	Degree of Freedom
LMD	Link Motion Disturbance
DCRA	Dexterous Collaborative Robot Arm
RTD	Robustness to Total Disturbance
TCP	Tool Center Point

REFERENCES

ALBU-SCHäFFER, A. & HIRZINGER, G. 2001. A globally stable state feedback controller for flexible joint robots. *Advanced Robotics,* 15**,** 799-814.

ALBU-SCHAFFER, A., OTT, C. & HIRZINGER, G. A passivity based cartesian impedance controller for flexible joint robots-part II: Full state feedback, impedance design and experiments. Robotics and Automation, 2004. Proceedings. ICRA'04. 2004 IEEE International Conference on, 2004. IEEE, 2666-2672.

ALBU-SCHäFFER, A., OTT, C. & HIRZINGER, G. 2007. A unified passivity-based control framework for position, torque and impedance control of flexible joint robots. *The International Journal of Robotics Research,* 26**,** 23-39.

ANDERSON, R. J. Dynamic damping control: Implementation issues and simulation results. Robotics and Automation, 1990. Proceedings., 1990 IEEE International Conference on, 1990. IEEE, 68-77.

CHENG, G., HYON, S.-H., MORIMOTO, J., UDE, A., HALE, J. G., COLVIN, G., SCROGGIN, W. & JACOBSEN, S. C. 2007. CB: A humanoid research platform for exploring neuroscience. *Advanced Robotics,* 21**,** 1097-1114.

DE LUCA, A. & LANARI, L. Robots with elastic joints are linearizable via dynamic feedback. Decision and Control, 1995., Proceedings of the 34th IEEE Conference on, 1995. IEEE, 3895-3897.

DE LUCA, A. & LUCIBELLO, P. A general algorithm for dynamic feedback linearization of robots with elastic joints. Robotics and Automation, 1998. Proceedings. 1998 IEEE International Conference on, 1998. IEEE, 504-510.

FIALA, J. & WAVERING, A. J. 1992. Experimental evaluation of Cartesian stiffness control on a seven degree-of-freedom robot arm. *Journal of Intelligent and Robotic Systems,* 5**,** 5-24.

GAO, Z. Active disturbance rejection control: a paradigm shift in feedback control system design. American Control Conference, 2006, 2006a. IEEE, 7 pp.

GAO, Z. Scaling and bandwidth-parameterization based controller tuning. Proceedings of the American control conference, 2006b. 4989-4996.

HAN, J. 2009. From PID to active disturbance rejection control. *IEEE transactions on Industrial Electronics,* 56**,** 900-906.

HASHIMOTO, M., HORIUCHI, T., KIYOSAWA, Y. & HIRABAYASHI, H. The effects of joint flexibility on robot motion control based on joint torque positive feedback. Robotics and Automation, 1991. Proceedings., 1991 IEEE International Conference on, 1991. IEEE, 1220-1225.

HOGAN, N. Impedance control: An approach to manipulation. American Control Conference, 1984, 1984. IEEE, 304-313.

HOLLERBACH, J., HUNTER, I., LANG, J., UMANS, S., SEPE, R., VAALER, E. & GARABIETA, I. The McGill/MIT direct drive motor project. Robotics and Automation, 1993. Proceedings., 1993 IEEE International Conference on, 1993. IEEE, 611-617.

HUANG, Y. & XUE, W. 2014. Active disturbance rejection control: methodology and theoretical analysis. *ISA transactions,* 53**,** 963-976.

HUNTER, I. W., HOLLERBACH, J. M. & BALLANTYNE, J. 1991. A comparative analysis of actuator technologies for robotics. *Robotics Review,* 2**,** 299-342.

HUR, S.-M., KIM, S.-K., OH, Y. & OH, S.-R. Joint torque servo of a high friction robot manipulator based on time-delay control with feed-forward friction compensation. RO-MAN, 2012 IEEE, 2012. IEEE, 37-42.

KAWAI, Y., YOKOKURA, Y., OHISHI, K. & SAITO, K. Equivalence of resonance ratio and I-PD controllers in zero stiffness torque control for soft robot. IECON 2015 - Conference of the IEEE Industrial Electronics Society, 2015. 001424-001429.

KAWAI, Y., YOKOKURA, Y., OHISHI, K., SAITO, K. & SHIMAMOTO, A. High back-drivable pseudo I-PD torque control using load-side torque observer with torsion torque sensor. IEEE International Workshop on Advanced Motion Control, 2016. 167-172.

KELLY, R. 1997. PD control with desired gravity compensation of robotic manipulators: a review. *The International Journal of Robotics Research,* 16**,** 660-672.

KELLY, R. & LLAMAS, J. Determination of viscous and Coulomb friction by using velocity responses to torque ramp inputs. Robotics and Automation, 1999. Proceedings. 1999 IEEE International Conference on, 1999. IEEE, 1740-1745.

KHALIL, H. K. 2014. *Nonlinear Control*, Pearson.

LUH, J., FISHER, W. & PAUL, R. 1983. Joint torque control by a direct feedback for industrial robots. *IEEE Transactions on Automatic Control,* 28**,** 153-161.

MASON, M. T. 1981. Compliance and force control for computer controlled manipulators. *IEEE Transactions on Systems, Man, and Cybernetics,* 11**,** 418-432.

MILLS, J. K. 1992. Stability and control of elastic-joint robotic manipulators during constrained-motion tasks. *IEEE Transactions on Robotics & Automation,* 8**,** 119-126.

OTT, C., ALBU-SCHAFFER, A. & HIRZINGER, G. Comparison of adaptive and nonadaptive tracking control laws for a flexible joint manipulator. Intelligent Robots and Systems, 2002. IEEE/RSJ International Conference on, 2002. IEEE, 2018-2024.

OTT, C., ALBU-SCHAFFER, A., KUGI, A., STAMIGIOLI, S. & HIRZINGER, G. A passivity based cartesian impedance controller for flexible joint robots-part I: Torque feedback and gravity compensation. Robotics and Automation, 2004. Proceedings. ICRA'04. 2004 IEEE International Conference on, 2004. IEEE, 2659-2665.

PAN, H., SUN, W., GAO, H. & JING, X. 2016. Disturbance observer-based adaptive tracking control with actuator saturation and its application. *IEEE Transactions on Automation Science and Engineering,* 13**,** 868-875.

PFEFFER, L. E., KHATIB, O. & HAKE, J. 1989. Joint torque sensory feedback in the control of a PUMA manipulator. *IEEE Transactions on Robotics and Automation,* 5**,** 418-425.

PRATT, G. A. & WILLIAMSON, M. M. Series elastic actuators. International Conference on Intelligent Robots and Systems, 1995. 399.

PRZYBYŁA, M., KORDASZ, M., MADOŃSKI, R., HERMAN, P. & SAUER, P. 2012. Active Disturbance Rejection Control of a 2DOF manipulator with significant modeling uncertainty. *Bulletin of the Polish Academy of Sciences: Technical Sciences,* 60**,** 509-520.

REN, T., DONG, Y., WU, D., WANG, G. & CHEN, K. Joint Torque Control of a Collaborative Robot Based on Active Disturbance Rejection With the Consideration of Actuator Delay. ASME 2017 International Mechanical Engineering Congress and Exposition, 2017. V04AT05A010.

REN, T., DONG, Y., WU, D., WANG, G. & CHEN, K. 2018. Collision detection and identification for robot manipulators based on extended state observer. *Control Engineering Practice,* 79**,** 144-153.

RIVIN, E. I. Effective rigidity of robot structures: Analysis and enhancement. American Control Conference, 1985, 1985. IEEE, 381-382.

SHAO, S. & GAO, Z. 2016. On the conditions of exponential stability in active disturbance rejection control based on singular perturbation analysis. *International Journal of Control***,** 1-13.

SPONG, M. W. 1987. Modeling and control of elastic joint robots. *Journal of dynamic systems, measurement, and control,* 109**,** 310-319.

SPONG, M. W. 1989. Adaptive control of flexible joint manipulators. *Systems & Control Letters,* 13**,** 15-21.

SWEET, L. M. & GOOD, M. C. Re-definition of the robot motion control problem: Effects of plant dynamics, drive system constraints, and user requirements. Decision and Control, 1984. The 23rd IEEE Conference on, 1984. IEEE, 724-732.

TIAN, L. & GOLDENBERG, A. A. Robust adaptive control of flexible joint robots with joint torque feedback. Robotics and Automation, 1995. Proceedings., 1995 IEEE International Conference on, 1995. IEEE, 1229-1234.

TOWNSEND, W. & SALISBURY, J. The effect of coulomb friction and stiction on force control. Robotics and Automation. Proceedings. 1987 IEEE International Conference on, 1987. IEEE, 883-889.

VALLERY, H., VENEMAN, J., ASSELDONK, E. V., EKKELENKAMP, R., BUSS, M. & KOOIJ, H. V. D. 2008. Compliant actuation of rehabilitation robots. *IEEE Robotics & Automation Magazine,* 15**,** 60-69.

VAN DER SCHAFT, A. 2016. *L2-gain and passivity techniques in nonlinear control*, Springer.

WANG, Q. G., LEE, T. H., FUNG, H. W., BI, Q. & ZHANG, Y. 1999. PID tuning for improved performance. *IEEE Transactions on Control Systems Technology,* 7**,** 457-465.

WU, C.-H. 1985. Compliance control of a robot manipulator based on joint torque servo. *The International journal of robotics research,* 4**,** 55-71.

WU, D., CHEN, K. & WANG, X. 2007. Tracking control and active disturbance rejection with application to noncircular machining. *International Journal of Machine Tools and Manufacture,* 47**,** 2207-2217.

XUE, W., BAI, W., YANG, S., SONG, K., HUANG, Y. & XIE, H. 2015. ADRC with adaptive extended state observer and its application to air–fuel ratio control in gasoline engines. *IEEE Transactions on Industrial Electronics,* 62**,** 5847-5857.

YANG, X. & HUANG, Y. Capabilities of extended state observer for estimating uncertainties. American Control Conference, 2009. ACC'09., 2009. IEEE, 3700-3705.

ZHOU, W., SHAO, S. & GAO, Z. 2009. A stability study of the active disturbance rejection control problem by a singular perturbation approach. *Applied Mathematical Sciences,* 3**,** 491-508.

ZHU, W.-H. & DE SCHUTTER, J. 1999. Adaptive control of mixed rigid/flexible joint robot manipulators based on virtual decomposition. *IEEE Transactions on Robotics and Automation,* 15**,** 310-317.